TISSUE ENGINEERING: Part A
Volume 23, Numbers 19 and 20, 2017

DOI: 10.1089/ten.tea.2016.0304

termis
Tissue Engineering
& Regenerative Medicine
International Society

SPECIAL FOCUS: STRATEGIC DIRECTIONS IN IMMUNORESPONSIVE BIOMATERIALS IN TISSUE ENGINEERING*

The Scaffold Immune Microenvironment: Biomaterial-Mediated Immune Polarization in Traumatic and Nontraumatic Applications

Kaitlyn Sadtler, PhD,[1,3] Brian W. Allen, BS,[1] Kenneth Estrellas, MS,[1] Franck Housseau, PhD,[2,3] Drew M. Pardoll, MD, PhD,[2,3] and Jennifer H. Elisseeff, PhD[1,3]

The immune system mediates tissue growth and homeostasis and is the first responder to injury or biomaterial implantation. Recently, it has been appreciated that immune cells play a critical role in wound healing and tissue repair and should thus be considered potentially beneficial, particularly in the context of scaffolds for regenerative medicine. In this study, we present a flow cytometric analysis of cellular recruitment to tissue-derived extracellular matrix scaffolds, where we quantitatively describe the infiltration and polarization of several immune subtypes, including macrophages, dendritic cells, neutrophils, monocytes, T cells, and B cells. We define a specific scaffold-associated macrophage (SAM) that expresses $CD11b^{+}F4/80^{+}CD11c^{+/-}CD206^{hi}CD86^{+}MHCII^{+}$ that are characteristic of an M2-like cell ($CD206^{hi}$) with high antigen presentation capabilities ($MHCII^{+}$). Adaptive immune cells tightly regulate the phenotype of a mature SAM. These studies provide a foundation for detailed characterization of the scaffold immune microenvironment of a given biomaterial scaffold to determine the effect of scaffold changes on immune response and subsequent therapeutic outcome of that material.

Keywords: extracellular matrix, macrophages, T cells, biomaterial implant, immune polarization

Introduction

Biomaterials are the foundation of therapeutics ranging from medical implants, sophisticated electronic devices, and scaffolds for regenerative medicine.[1,2] While historic approaches to biomaterial design centered on minimizing interactions with the body, today's strategies focus on creating materials that are biointeractive and more specifically shape the local protein, cell, and tissue environment to guide biological responses.[3]

For example, in the case of glucose sensors, vascular integration is promoted to optimize blood sensing,[4–6] while neuronal integration is desired for transmission of signals in implanted electrodes.[7] Medical implants such as hip and knee prosthetics are coated to enhance bone integration and implant stability,[8] whereas breast implants should integrate with surrounding soft tissue and avoid a foreign body response that encases and hardens the prosthetic.[9] Finally, scaffolds for regenerative medicine are also designed to interface with surrounding biology to promote functions such as cell infiltration, adhesion, and proliferation to ultimately stimulate tissue morphogenesis.

When any of the materials in devices or scaffolds are implanted in the body, the immune system is the first responder to both the trauma of implantation and the foreign body itself. Synthetic biomaterials primarily induce a foreign body response that eventually forms a fibrous capsule around the material, while biological scaffolds are not as susceptible to such encapsulation and are often integrated with the surrounding tissue.[10–12] The biophysical and biochemical properties of the material and the location of implantation will all impact the type and function of immune response.[3] Advances in immunology and immune cell phenotypic characterization now allow exquisitely detailed understanding of an immune response that can also be applied to understand, and in the future manipulating and controlling, the immune response to biomaterials.[13]

[1]Translational Tissue Engineering Center, Department of Biomedical Engineering, Johns Hopkins University School of Medicine, Baltimore, Maryland.
[2]Sidney Kimmel Comprehensive Cancer Center, Department of Oncology, Johns Hopkins University School of Medicine, Baltimore, Maryland.
[3]Bloomberg ~ Kimmel Institute for Cancer Immunotherapy, Johns Hopkins University School of Medicine, Baltimore, Maryland.

*This article is part of a special focus issue on Strategic Directions in Immunoresponsive Biomaterials in Tissue Engineering. An additional article can be found in Tissue Engineering Part B, volume 23, number 5.

The immune system surveys the body for disruptions in homeostasis. Application of a biomaterial, in the presence or absence of trauma, will initiate recruitment of immune cells.[10,14] For decades, this immune response was viewed as a destructive phenomenon that ultimately ended in either fibrous capsule formation or inflammation and scaffold degradation.[15–18] Therefore, for device development, research involved the protection of biomaterials from the immune response and decreasing recognition of the materials as foreign material to create a more regulatory response that would not lead to inflammation or fibrosis.[19,20] The field of regenerative medicine has evolved toward biointeractive material design; however, the complexity of the immune response has remained a critical variable that has not been fully integrated.

These complexities include both the number of different cell types and mechanisms of detection that the immune system employs, as well as the specificity of the response that creates a different immune environment dependent upon tissue location. Every tissue has a unique immunologic steady state and tendencies toward certain polarization states,[21,22] or even a lack of a robust immune response, such as immune-privileged sites like the cornea, neural tissue, and testes.[23]

The immune system can impact many processes in the body ranging from defense against bacteria and viruses to embryonic development. There are cells of the immune system throughout the body that can relay a signal of tissue damage or in the case of biomaterials, their implantation. In the case of injury, immune cells are critical for wound healing and tissue regeneration.[24–32]

Previously, researchers have noted the importance of macrophages in complex tissue regeneration in amphibians[33] and muscle regeneration in higher organisms.[34] Eosinophils, macrophages, and T cells have been implicated in regenerative processes.[13,35] In addition, macrophages are important in the outcome of biologic scaffold remodeling, specifically tissue-derived extracellular matrix (ECM) scaffolds.[11,36–40] Biochemically, macrophages, among other cells, secrete enzymes responsible for ECM remodeling in normal and diseased conditions.[41,42] This is especially important in tissue engineering, as the host must be able to successfully incorporate and remodel the scaffold into a functional replacement tissue.

We developed a multiparameter flow cytometry analytic approach to appreciate the complexity of recruitment and polarization of immune cells in response to biomaterial scaffolds in nontraumatic (subcutaneous) and traumatic (muscle injury) models. Flow cytometric analysis of the scaffold immune microenvironment (SIM) revealed the presence of a specific set of scaffold-associated macrophages (SAMs) with a surface profile of $CD11b^{+}F4/80^{+}CD11c^{+/-}CD206^{hi}CD86^{+}MHCII^{+}$. In addition, we observed an adaptive immune-dependent MHCII and CD11c upregulation by scaffolds in the volumetric muscle injury model. With more thorough characterization and better understanding of the immune response to biomaterials and the SIM, biomaterials can be improved with a more rational design.

Materials and Methods

Tissue decellularization

Tissues were derived from porcine (Wagner Meats) and decellularized following a standard protocol.[13,43] Briefly, samples were diced into small pieces using a knife-mill processor (Retsch, Germany), no larger than 2 mm^2, and rinsed thoroughly with running distilled water until blood was cleared from tissue. Bone samples were pretreated for decalcification by incubation in 10% formic acid (Sigma-Aldrich) for 3 days, verified by a colorimetric calcium test (Stanbio). Tissues were then incubated in 3.0% peracetic acid (Sigma-Aldrich) on a shaker at 37°C, 400 rpm for 4 h, changing the solution after 1 h to fresh acid. pH was equilibrated by successive rinses with phosphate-buffered saline (PBS; Life Technologies) until reaching 7 according to colorimetric pH paper. Samples were transferred to a 1% Triton-X100 (Sigma-Aldrich) + 2 mM sodium EDTA solution on a stir plate (400 rpm) at room temperature for 3 days, changing the solution daily. Tissues were rinsed thoroughly with distilled water until there were no bubbles forming from detergent. Finally, they were incubated in 600 U/mL DNase I (Roche Diagnostics) + 10 mM $MgCl_2$ + 10% Antifungal-Antimycotic (Gibco®) for 24 h. Tissues were rinsed with distilled water, then frozen at −80°C and lyophilized for 2 days. The dry sample was cryogenically milled into a particulate form using SPEX SamplePrep Freezer/Mill (SPEX SamplePrep).

Subcutaneous ECM implantation

ECM was hydrated with 1× PBS to form implants of 300 mg/mL. Using an 18G needle, 200 μL of the ECM paste was injected twice subcutaneously into female 6-week-old wild-type C57BL/6 mice (Charles River Laboratories), both cranial and caudal locations. Hair was removed with an electric razor and skin was sterilized with ethanol and Povidone-Iodine. Implants were dissected with surrounding tissue and processed for histology and flow cytometry (FACS). All animal procedures were done in accordance with the Johns Hopkins University ACUC guidelines.

Volumetric muscle loss surgery

Six- to 8-week-old female C57BL/6 (Charles River Laboratories) or B6.129S7.*Rag1*^{tm1Mom}/J (*Rag1*$^{-}$; Jackson Laboratories) were induced under 4.0% isoflurane and maintained at 2–3.0% isoflurane and 2% O_2 during the surgery. Both hind limbs were cleared of hair using an electric razor. Skin was sterilized with 70% ethanol before surgery. A 1-cm incision was created above the quadriceps muscle using surgical scissors. The underlying fascia was cut and the inguinal fat pad was pushed toward the hip joint to reveal the quadriceps muscle group. Using surgical scissors, a 3 × 4 mm portion of muscle was removed and back-filled with either saline or 50 μL of a 200–300 mg/mL particulate biomaterial. The skin incision was closed with surgical staples and the procedure was repeated on the contralateral leg. Before removal from anesthesia, animals were given 5 mg/kg carprofen (Rimadyl®; Zoetis) for pain management. For the duration of the study, animals were maintained under Uniprim® antibiotic feed (275 ppm trimethoprim and 1365 ppm sulfadiazine; Harlan Laboratories) until the end of study. On day 7 postinjury, the scaffold and surrounding muscle were harvested for FACS analysis by running a scalpel blade from the knee along the femur to the hip joint and finely dicing the muscle and scaffold before proceeding with enzyme digestion as described in the Flow Cytometry methods section. All animal procedures were done in accordance with the Johns Hopkins University ACUC guidelines.

Histology

Implants were fixed for 48 h at room temperature in 10% formalin before dehydration and paraffin embedding. Five-micrometer sections were rehydrated and then prepared for immunohistochemistry (IHC) or direct staining with hematoxylin and eosin (Sigma-Aldrich). IHC samples were treated with a citrate antigen retrieval buffer, 10 mM sodium citrate (J.T. Baker) + 0.05% Tween 20 (Sigma-Aldrich) at pH 6, for 30 min in a vegetable steamer. Sections were stained with primary antibodies against CD11b, CD3, neutrophil elastase, or CD11c (AbCam) overnight at 4°C and then visualized using the SuperPicture™Polymer Detection Kit, HRP-DAB (Life Technologies). These samples were then counterstained with hematoxylin (Sigma-Aldrich).

Flow cytometry

Subcutaneous ECM implants and muscle samples were harvested and then finely diced using a scalpel in 1× PBS. Resultant material was digested for 45 min at 37°C on a shaker at 400 rpm in 0.5 mg/mL Liberase TL (Roche Diagnostics) + 0.2 mg/mL DNase I (Roche Diagnostics) in serum-free RPMI (Gibco). Digest was filtered through a 100 μm cell strainer and then washed twice with 1× PBS. Cells were re-suspended in 5 mL 1× PBS and carefully layered atop 5 mL Lympholyte-M (Cedarlane), and then spun for 20 min at 1200 *g*. Cellular interphase was washed twice with 1× PBS and then transferred to a 96-well plate for antibody staining. Isolated cells were stained with the following antibody panel: LIVE/DEAD® Fixable Aqua (Cat #L34957; Life Technologies), CD19 BrilliantViolet 421 (Cat #115537; BioLegend), CD3 AlexaFluor 488 (Cat #100210; BioLegend), CD11c APC/Cy7 (Cat #561241; BD Biosciences), F4/80 PE/Cy7 (Cat #123113; Biolegend), CD86 AlexaFluor700 (Cat #105024; BioLegend), and CD206 APC (Cat #141708; BioLegend). After staining, cells were fixed and analyzed as previously described. Viability Aqua negative (live) cells were evaluated based on percent population of T cells ($CD3^+$), B cells ($CD19^+$), dendritic cells ($CD11c^+$), and macrophages ($F4/80^+$). All analyses were performed in FlowJo Flow Cytometry Analysis Software (Treestar). T cell analysis was performed using the following panel: CD3 AlexaFluor488 (Cat #100210; Biolegend), CD4 PE/Cy7 (Cat #100422; Biolegend), CD8α AlexaFluor700 (Cat #100730; Biolegend), FoxP3 Pacific Blue (Cat #126410; Biolegend), and Fixable Viability Dye eFluor®780 (Cat #65-0865; eBioscience). Myeloid compartment analysis in the volumetric muscle wound at 1 week postinjury was done with the following antibody panel: Fixable Viability Dye eFluor780 (Cat #65-0865; eBioscience), F4/80 PE/Cy7 (Cat #123113; BioLegend), CD11b AlexaFluor700 (Cat #101222; BioLegend), CD11c APC (Cat #117310; BioLegend), Ly6C PerCP/Cy5.5 (Cat #128011; BioLegend), Ly6G PacificBlue (Cat #127612; BioLegend), CD86 BrilliantViolet510 (Cat #105039; BioLegend), and CD206 PE (Cat #141705; BioLegend), MHCII I-A/I-E AlexaFluor488 (Cat #107616; BioLegend).

Statistical analysis

Analysis of variance (ANOVA) and Student's *t*-tests were performed using Prism GraphPad software at $p \leq 0.05$. In cases where ANOVA was used and multiple comparisons were made, Tukey's *post hoc* test for multiple comparisons was applied.

Results

Subcutaneous implantation of ECM biomaterials derived from various tissue sources

To model the immune response to ECM scaffolds in a nontraumatic setting, we injected 0.2 cc of a 300 mg/mL ECM scaffold subcutaneously in wild-type C57BL/6 mice. After 1 and 3 weeks, the implants were harvested for analysis by histology. In all tissue sources tested (Bone, Cardiac, Liver, Lung, and Spleen), a 100 to 200 micron fibrous capsule and cellular infiltrate formed around the implant by 1 week postinjection (Fig. 1A), which thickened and increased in cellularity by 3 weeks postinjection (Fig. 1B). Implants decreased in size over time from 1 to 3 weeks as the scaffold was being degraded and remodeled (Fig. 1A, B). Dense cellular tissue was detected both at the skin (dorsal) and capsular (ventral) interfaces with cellular infiltration in most implants through the center by 1 week postinjection (Fig. 1C). There was not a significant difference in capsule thickness (Fig. 1D) or intraimplant cellularity (Fig. 1E) between the various tissue ECM sources.

Further characterization of the immune infiltrate was achieved by staining for cells of the innate (macrophages, dendritic cells) and adaptive (T cells) immune system. The immune response to subcutaneous scaffolds was dominated by $CD11b^+$ macrophages with scattered $CD11c^+$ dendritic cells and a large number of $CD3^+$ T cells (Fig. 2). Most macrophages occupied the capsule including dense clusters of cells at the skin interface (Fig. 2A, B) with minimal CD11b staining in the more central regions. Dendritic cells were found in the dermis, characteristic of resting Langerhans cells, as well as at the skin and capsular interfaces. These cells were excluded from the clusters containing $CD11b^+$ macrophages. $CD3^+$ T cells were found surrounding the implant much like macrophages and dendritic cells, and were densely present around vascular structures (Fig. 2A, Bone CD3). In addition, T cells colocalized with $CD11b^+$ macrophages in cellular aggregates at the skin interface (Fig. 2B). The clustering of macrophages and T cells, but not dendritic cells, suggests communication between T cells and macrophages as opposed to the canonical communication with dendritic cells (Fig. 2C).

Multiparameter flow cytometric analysis of the SIM

The SIM was characterized by flow cytometry (FACS) analysis of freshly enzymatically digested tissue (Figs. 3 and 4). We confirmed the presence of T cells, dendritic cells, and macrophages first observed in histological staining (Fig. 3). B cells were also detected (Fig. 3). There was a statistically significant variation in immune response dependent on scaffold source. Recruitment of T cells and B cells was more prominent at 3 weeks (Fig. 3B, C), suggesting induction of acquired immune responses. The overall SIM profile was similar between scaffolds with a high proportion of myeloid cells (>25% of total infiltrate) followed by $CD3^+$ T cells (3–5%) and minimal levels of $CD19^+$ B cells (<0.1%). By 3 weeks, the overall immune profile was significantly different

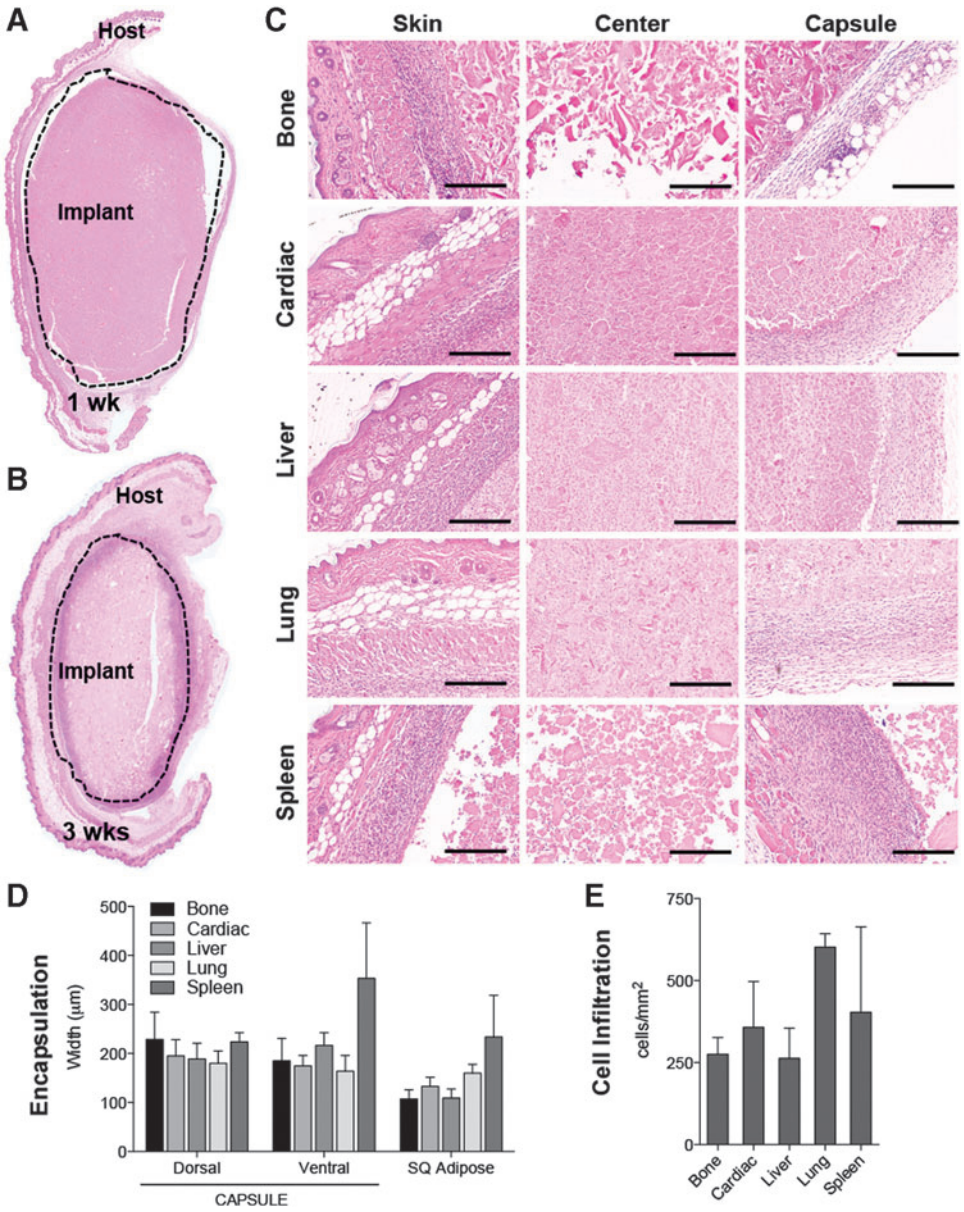

FIG. 1. Subcutaneous injection of particulate ECM scaffolds induces cellular encapsulation and infiltration. **(A)** H&E composite image of 1 week postinjection, liver ECM implant. **(B)** Composite image of 3 weeks postinjection, lung ECM implant. **(C)** High magnification of skin (dorsal) and capsule (ventral) interfaces and center of implant. **(D)** Quantification of the capsule/cellular infiltrate front width and subcutaneous fat pad width in microns at 1 week postinjection. **(E)** Cellular infiltration within implant displayed as cell count per mm^2. Scale bars = 200 μm. Data are mean ± SEM, $n = 4$. ECM, extracellular matrix; H&E, hematoxylin and eosin; SEM, standard error of the mean.

between the tissue sources; however, the general pattern of infiltrate remained the same (Fig. 3C).

As the M1/M2 axis of macrophage polarization has been associated with scaffold remodeling, wound healing, and tissue regeneration, we further characterized myeloid cells present in the SIM. Myeloid cells were by their expression of CD86 (costimulatory molecule in antigen presentation; M1 marker) and CD206 (mannose receptor; M2 marker). Three distinct myeloid cell populations were present and varied in their CD86/CD206 expression. SAMs were $F4/80^{+}CD86^{+}CD206^{hi}$ (Fig. 4, Supplementary Fig. S1, Supplementary Table S1; Supplementary Data are available online at www.liebertpub.com/tea). Mature macrophages ($F4/80^{hi}$) expressed higher levels of CD206 and CD86 than $F4/80^{lo}$ macrophages. Dendritic cells ($CD11c^{+}$) did not express CD206, but had high levels of CD86 expression. $CD11c^{+}F4/80^{+}$ macrophages expressed high levels of both CD86 and CD206 ($CD86^{hi}CD206^{+}$). ECM scaffolds induced a mixed M1/M2 phenotype and the SAMs expressed both the M1 and M2 markers (CD86 and CD206). Further dissection of the myeloid compartment could reveal more specific subtypes present in the subcutaneous SIM.

In addition, implants were analyzed by multiparameter flow cytometry to determine the presence of more specific T cell subtypes based on their expression of CD4 (helper T cells), CD8 (cytotoxic T lymphocytes), and FoxP3 (regulatory T cells) (Fig. 5). In these more detailed studies, we used ECM derived from bone and cardiac muscle. These two tissues represent very different sources of ECM: bone, a tissue that is ECM dense and has minimal cells, versus cardiac muscle, a tissue with minimal amounts of ECM and high cellular material. Helper T cells were the most abundant $CD3^{+}$ T cell subtype in both scaffolds tested (>60% of $CD3^{+}$) compared to $CD8^{+}$ cytotoxic T lymphocytes (<15% of $CD3^{+}$) (Fig. 5B). Cardiac ECM recruited slightly skewed the ratio of CD4 to CD8 T cells. Both scaffolds recruited $FoxP3^{+}$ T cells, but bone ECM recruited far more than cardiac ECM (24.13 ± 4.33 vs. 1.24 ± 0.22, $p = 0.0019$, Fig. 5C).

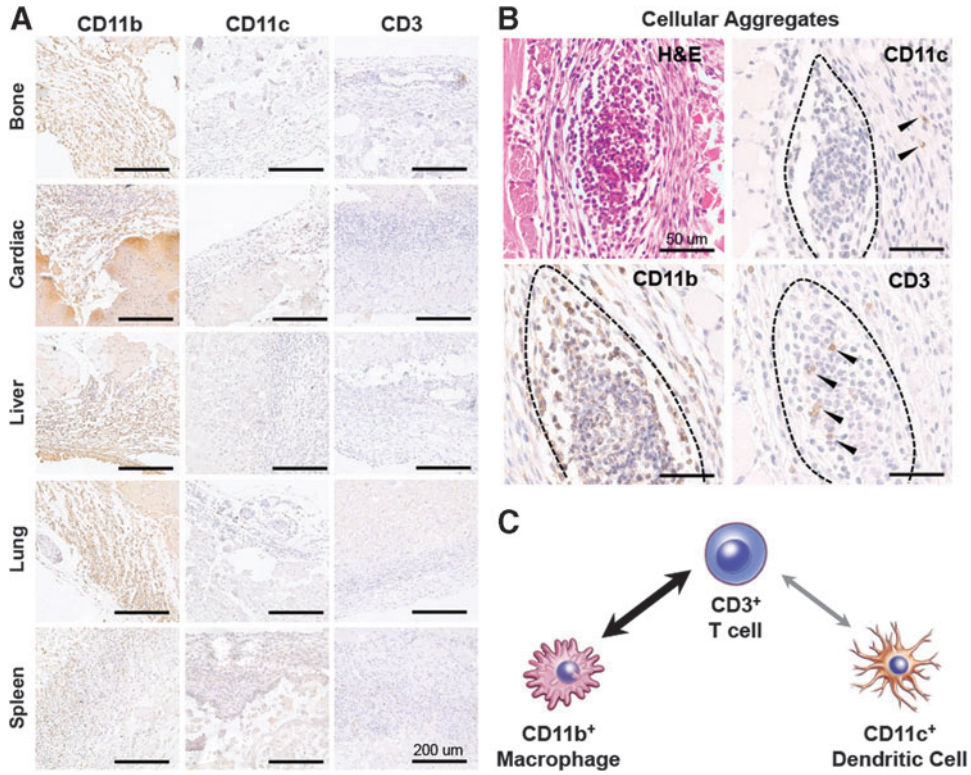

FIG. 2. Immune response to scaffolds is dominated by $CD11b^+$ macrophages communicating with $CD3^+$ T cells. **(A)** Immunohistochemical staining of the dorsal (skin) interface of the implant for $CD11b^+$ macrophages, $CD11c^+$ dendritic cells, and $CD3^+$ T cells. **(B)** Cellular aggregates present at the dorsal interface stain positive for CD11b and CD3, but exclude CD11c. **(C)** Colocalization of $CD11b^+$ macrophages and $CD3^+$ T cells suggests an increased communication between macrophages and T cells as opposed to canonical $CD11c^+$ dendritic cells. Scale bars = 200 μm.

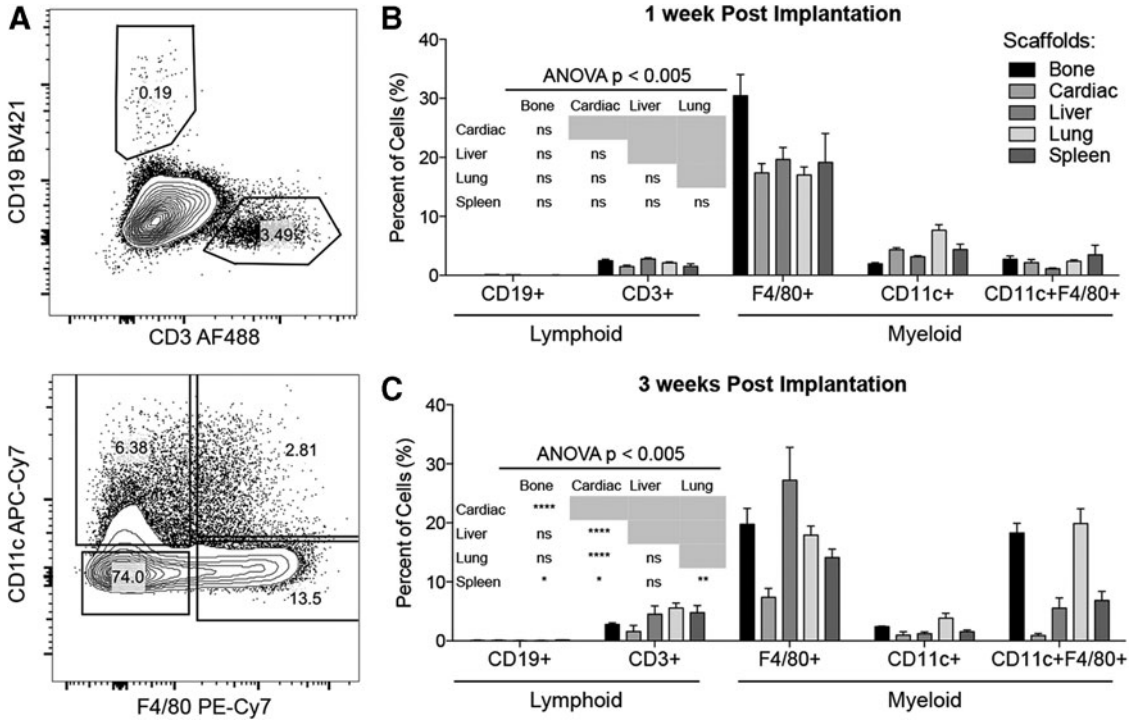

FIG. 3. Immune infiltrate profile depends on tissue source and time postinjection. **(A)** Six-color flow cytometry was used to define the lymphoid compartment: $CD3^+$ T and $CD19^+$ B cells and the myeloid compartment: $F4/80^+$ macrophages and $CD11c^+$ dendritic cells. **(B)** Immune profile at 1 week postinjection. **(C)** Immune profile at 3 weeks postinjection. Data are mean ± SEM, $n = 4$. Significance determined by ANOVA with Tukey's *post hoc* correction for multiple comparisons. ANOVA, analysis of variance.

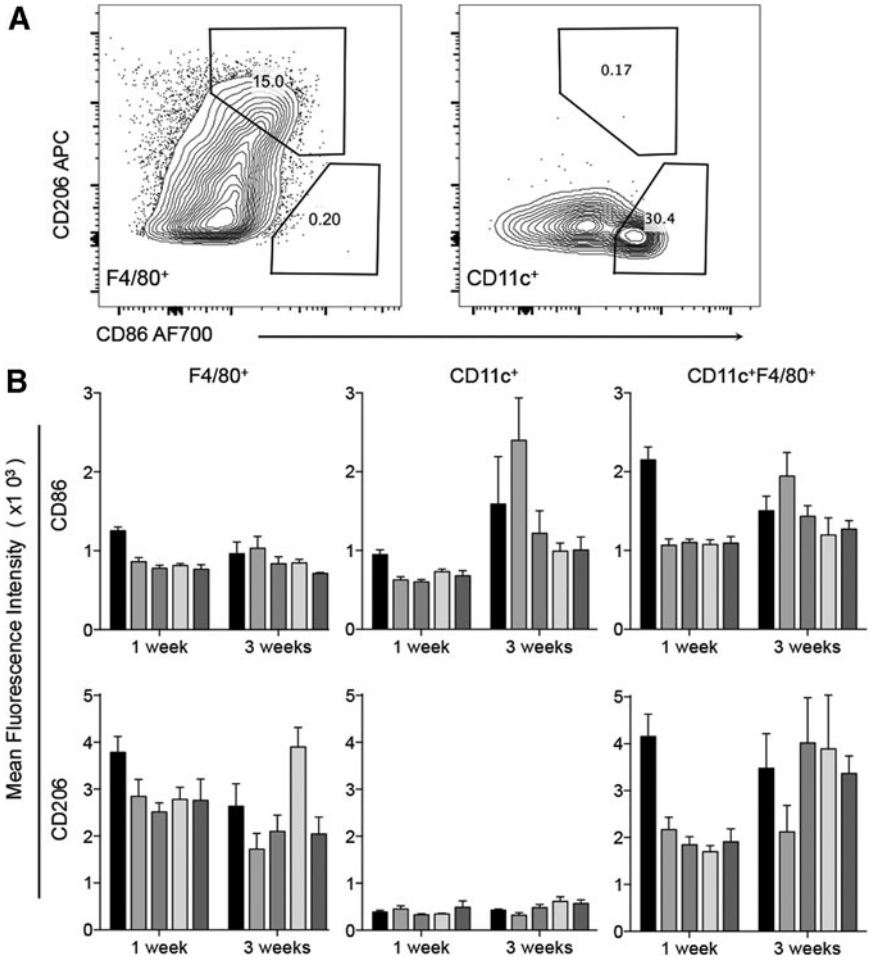

FIG. 4. Myeloid subtypes defined by F4/80, CD11c, CD206, and CD86 expression. F4/80$^+$ macrophages are CD86$^+$CD206^{hi}, CD11c$^+$ dendritic cells are CD86^{hi}CD206$^-$, and CD11c$^+$F4/80$^+$ macrophages are CD86^{hi}CD206$^+$. **(A)** Representative *dot* plots of CD86 and Cd206 expression in F4/80$^+$ macrophages and CD11c+ dendritic cells. **(B)** Quantification of data shown in **(A)**. Data are mean ± SEM, $n = 4$. Significance determined by ANOVA with Tukey's *post hoc* correction for multiple comparisons (Supplementary Fig. S1).

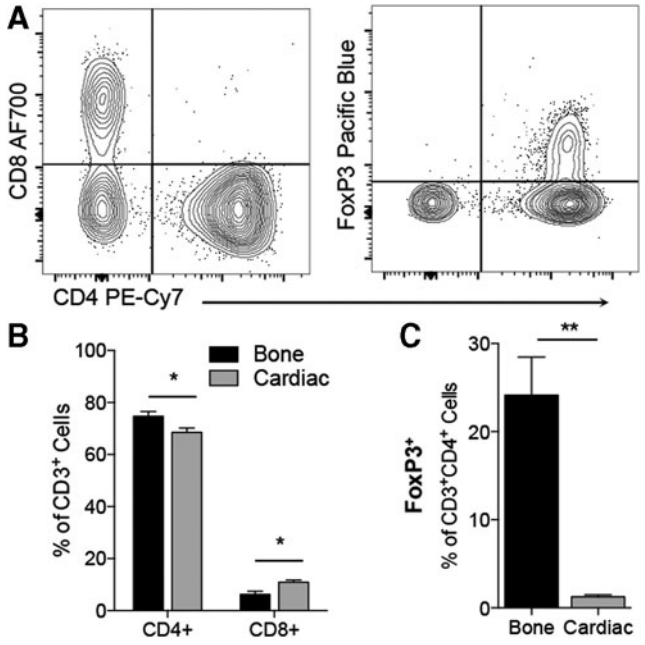

FIG. 5. T cell profile is dominated by CD4$^+$ T cells. **(A)** Representative plots of CD4 versus CD8 profile and FoxP3 gating. **(B)** CD4/CD8 ratio in bone- and cardiac-derived scaffolds. **(C)** FoxP3$^+$ T_{regs} are detected at higher levels in bone ECM than cardiac ECM. Data are mean ± SEM, $n = 4$. Significance determined by Student's *t*-test.

A scaffold-associated immune profile is detected in ECM-treated volumetric muscle wounds

ECM scaffolds have been used clinically to treat traumatic wounds such as skin lesions,[44] hernia repair,[45] and muscle loss.[40] To create a traumatic muscle wound, we used a murine volumetric muscle loss. After injury, mice received 50 μL of saline vehicle control, collagen, decalcified bone (B-ECM), or ventricular cardiac muscle (C-ECM) (Fig. 6A). At 7 days postinjury, the scaffold and surrounding musculature were harvested and prepared for analysis with flow cytometry. As this is an early injury response window, we stained for a comprehensive panel of innate immune cells, or myeloid cells. From this panel, we could detect F4/80$^+$CD11b$^+$ macrophages (Fig. 6B), CD11b$^{+/-}$F4/80$^-$CD11c$^+$ dendritic cells (Fig. 6C), CD11b$^+$Ly6c$^+$ immature monocytes and CD11b$^+$Ly6g$^+$ polymorphonuclear cells (Fig. 6D, PMNs; neutrophils, eosinophils, and basophils). In addition, we included markers for M1/M2 polarization (CD86 and CD206) and antigen presentation to CD4$^+$ T cells (MHCII I-A/I-E). Previously, we have demonstrated the critical role for adaptive immune cells, specifically CD4$^+$ Th2 T cells, in polarizing the SIM and promoting an M2-macrophage phenotype.[13] Therefore, we analyzed the myeloid profile of B6.129S7.*Rag1*^{tm1Mom}/J (*Rag1*$^{-/-}$) mice to further dissect the interactions of adaptive immune cells with the myeloid compartment of the SIM. As with previous studies, the SIM comprised a large proportion of F4/80$^+$CD11b$^+$ macrophages

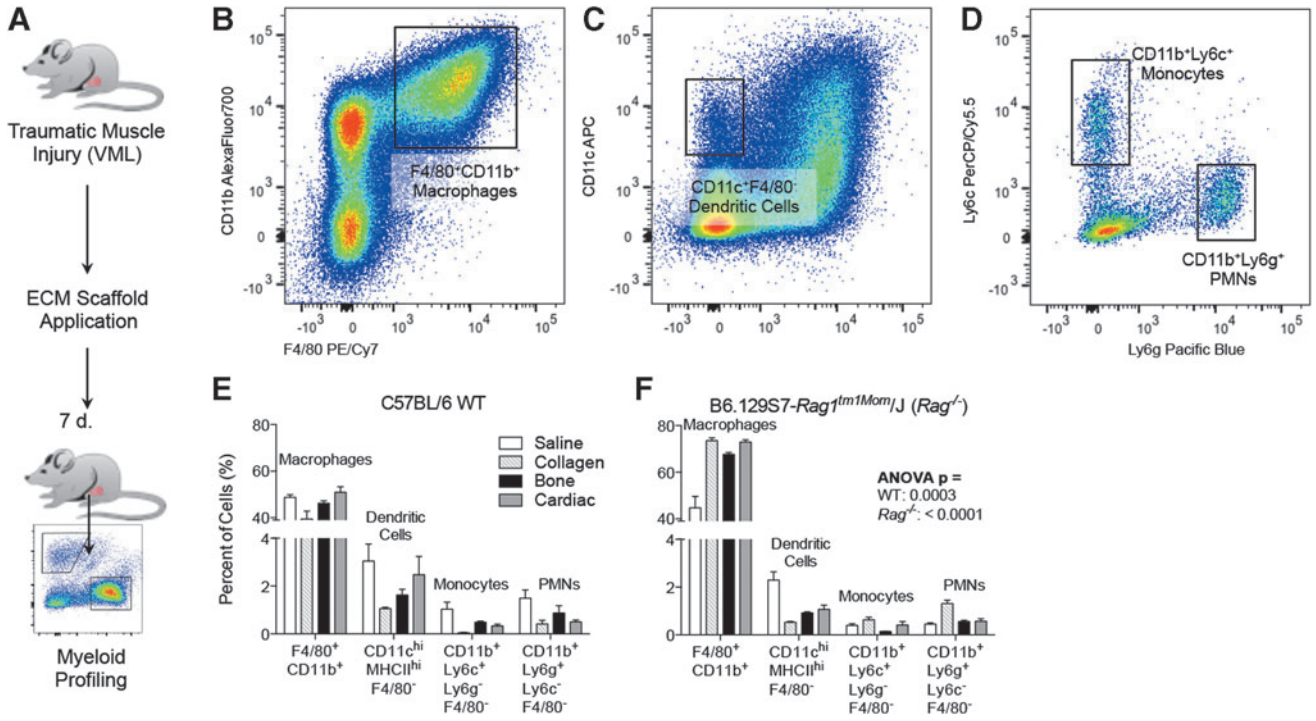

FIG. 6. Detailed profile of myeloid cells in a scaffold-treated volumetric muscle wound. **(A)** A 3×4 mm portion of the quadriceps muscle is excised and replaced with a biomaterial scaffold: Saline vehicle control, Collagen, B-ECM (decalcified bone ECM), and C-ECM (ventricular cardiac muscle-derived ECM). **(B)** $F4/80^{+}CD11b^{+}$ macrophage infiltrate. **(C)** $CD11c^{+}F4/80^{-}$ dendritic cell infiltrate. **(D)** $CD11b^{+}Ly6c^{+}$ (immature monocytes) or $Ly6g^{+}$ (polymorphonuclear cells; neutrophils, eosinophils, basophils). **(E, F)** Myeloid infiltrate in wild type (WT) **(E)** or *Rag1*$^{-/-}$ **(F)** mice, which lack mature T and B cells. Data shown for tissue-derived matrices (bone and cardiac ECM), collagen control, and saline vehicle control. Data are mean ± SEM, $n = 4$. Significance calculated by ANOVA.

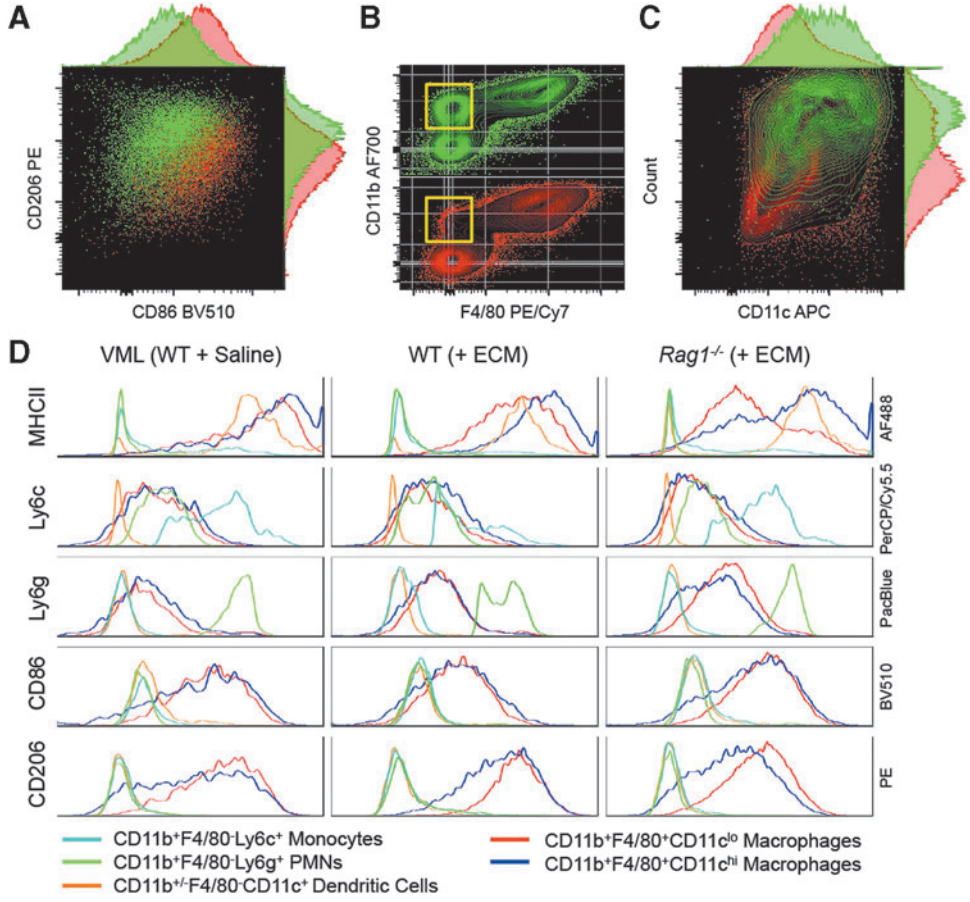

FIG. 7. Myeloid profile is dependent on scaffold and presence of adaptive immune cells. **(A)** Characteristic CD86 increase and CD206 decrease in the absence of adaptive immune cells (*Rag1*$^{-/-}$; *red*). **(B)** Decrease in $CD11b^{+}F4/80^{-}$ cells in *Rag1*$^{-/-}$ mice. **(C)** CD11c expression on $F4/80^{+}CD11b^{+}$ macrophages is dependent on adaptive immune cells. *Yellow box* outlines population of interest. **(D)** Multiparametric analysis of surface markers on different myeloid subtypes. Data shown for tissue-derived bone ECM (+ECM) and saline vehicle control. *Light blue line* = $CD11b^{+}F4/80^{-}Ly6c^{+}$ monocytes; *Green line* = $CD11b^{+}F4/80^{-}Ly6g^{+}$ polymorphonuclear cells (PMNs, neutrophils, basophils eosinophils); *Orange line* = $CD11b^{+/-}F4/80^{-}CD11c^{+}$ dendritic Cells; *Red line* = $CD11b^{+}F4/80^{+}CD11c^{lo}$ macrophages; *Blue line* = $CD11b^{+}F4/80^{+}CD11c^{hi}$ macrophages.

(40–50% at 1 week postinjury; Fig. 6E). *Rag1*$^{-/-}$ mice recruited a higher proportion of macrophages compared to wild type (WT) counterparts and fewer PMNs (Fig. 6F).

There was a characteristic adaptive immune-dependent M2-phenotype in F4/80^{+}CD11b^{+} macrophages with elevated CD206 and decreased CD86 at 1 week postinjury (Fig. 7A). As noted previously, *Rag1*$^{-/-}$ mice had an increased number of CD11b^{+}F4/80^{+} macrophages, which correlated with a decrease in CD11b^{+}F4/80^{-} myeloid cells, suggesting a possible differentiation or maturation of F4/80^{-} cells to F4/80^{+} macrophages (Fig. 7B). Interestingly, scaffold-mediated CD11c upregulation in CD11b^{+}F4/80^{+} macrophages is dependent upon adaptive immune cells (Fig. 7C, Supplementary Fig. S2). MHCII expression was highest on CD11c^{hi}CD11b^{+}F4/80^{+} macrophages followed by CD11b$^{+/-}$F4/80^{-}CD11c^{+} dendritic cells and CD11c^{lo}CD11b^{+}F4/80^{+} macrophages (Fig. 7D, Supplementary Figs. S3 and S4). As with CD86 and CD206 expression, the MHCII expression was dependent upon adaptive immune cells and decreased in *Rag1*$^{-/-}$ mice. PMNs, monocytes, and dendritic cells expressed low levels of CD86 and CD206 when compared to macrophages. Notably, there is a dramatic reduction of MHCII expression in the F4/80^{+}CD11c^{lo} macrophage population in the *Rag1*$^{-/-}$ mice, associated with an increase in immature monocytes (Ly6c^{+}), compared to the WT ECM-treated mice (Fig. 7D, Supplementary Fig. S4).

Discussion

Tissue microenvironment is an important determinant in host response to biomaterials used in tissue engineering, from differences in mechanical strain to differences in immune cells present to react with those materials. In immune responses to various challenges, such as pathogen-derived or biomaterial foreign body responses, this microenvironment plays a crucial role in shaping the reaction to fit the location in which it occurs.[21,22] In terms of the tissue environment, the stage can be seen orchestrated by the biomaterial and the location where the material is implanted. ECM scaffolds differ in their biochemical and structural composition, which are imbued by the tissue from which those ECM scaffolds are derived. These various tissue sources create scaffold microenvironments that can alter the polarization of the immune cells that migrate to that scaffold upon implantation. The immune cells that come to the implant will differ depending on the host tissue in which the material is implanted and the presence or absence of injury. These cells will be affected by the scaffold microenvironment, causing them to alter the signals that they in turn send back to the surrounding tissue. This cycle of interaction between the scaffold and host tissue environment, connected by the immune cells, will dictate the therapeutic capacity of that scaffold.[3]

Through histological examination, it is possible to determine the extent of cellularity as well as the locational distribution of cells from specific lineages. For example, we describe an abundance of CD11b^{+} macrophages that colocalize with CD3^{+} T cells in cellular aggregates at the skin interface. This suggests a communication of T cells with macrophages and possibly an activation of the adaptive immune system through this highly phagocytic cell type. To further define the SIM created by ECM scaffolds, we employed the use of multicolor flow cytometry. Flow cytometry (FACS) provides a method of high-throughput quantitative immune phenotyping. FACS is critical in fields such as tumor immunology where they study immune cell recruitment and polarization in tumors to determine the most efficacious immunotherapy techniques for cancer treatment. Just as tumor immunologists use FACS to define a tumor microenvironment, we used FACS to define the SIM. As with histological staining, we were able to detect macrophages, dendritic cells, and T cells, as well as B cells. By staining for CD86 (M1 marker) and CD206 (M2 marker), we were able to characterize the polarization of myeloid cells along the M1-M2 axis. Three myeloid cell types with different M1/M2 profiles were described. These include M1-like dendritic cells, M2-like macrophages, and CD11c^{+}F4/80^{+} myeloid cells that represent an intermediate phenotype expressing high levels of both CD86 and CD206.

Macrophage colocalization with T cells in cellular aggregates, found in the scaffold at the skin interface, suggests a possible communication with the adaptive immune system. Previously, researchers have shown that subcutaneous implants can induce a Th2-like phenotype.[46,47] Connecting the MHCII^{+} M2-macrophage phenotype with the knowledge of a Th2-associated ECM response, we can assume that there is communication between M2 macrophages and Th2 T cells in the SIM. We have defined a SAM that is F4/80^{+}CD11c$^{+/-}$ CD206^{hi}CD86^{+}MHCII^{+}. CD206^{+} SAMs could potentially be recognizing the fragmented ECM composed of proteins, proteoglycans, and polysaccharides that have been milled to a fine particulate. More specifically, CD206 can recognize *N*-acetylglucosamine, fucose, and mannose.[48,49] These ECM fragments in the scaffolds recapitulate the signals from damaged tissue that are produced in a wounding response and, therefore, can magnify the immune response to Damage Associated Molecular Patterns (DAMPs). In addition, CD206 and CD86 expression on SAMs is dependent upon the presence of adaptive immune cells.[13] In this study, we show that adaptive immune cells regulate CD11c expression on SAMs. CD11c is an integrin that is involved in the adherence of activated cells to the endothelium of blood vessels and binding of complement-coated cells and materials.[50] CD11c and CD206 are important sensors of the environment and can dictate the myeloid response to a scaffold or surrounding tissue. Also, the reduction of MHCII on CD11c^{lo} macrophages that is associated with the increase in Ly6c^{+} monocytes in *Rag1*$^{-/-}$ ECM-treated mice, demonstrates a decrease in myeloid maturation to tissue-resident macrophages and an accumulation of monocytes in the absence of adaptive immune cells. The overall fraction of CD11b^{+}F4/80^{+} macrophages is also disrupted in *Rag1*$^{-/-}$ mice, where the *Rag1*$^{-/-}$ animals have a larger proportion of CD11b^{+}F4/80^{+} macrophages and a decreased proportion of CD11b^{+}F4/80^{-} myeloid cells. This suggests that the adaptive immune cells are required for proper activation and recruitment of myeloid cells to the SIM.

Macrophages have been implicated in multiple aspects of immune response to biomaterials as well as the outcome of scaffold remodeling, where M2-type macrophages are critical in ECM scaffold remodeling.[11,38] In addition, macrophages have been associated with several developmental processes, including salamander limb regeneration.[33] Other immune cells, such as eosinophils and T cells, have been implicated in wound healing of higher organisms.[13,35] These connections between biomaterials, immune cells, and development are

important considerations for scaffold design to ensure that the biomaterial will promote regeneration through proper polarization of the immune response.

When analyzing cell recruitment and polarization in the context of biomaterials by flow cytometry, several factors must be addressed and acknowledged to ensure reliable data acquisition. For example, when digesting a tissue sample to isolate single cells, there are various enzymatic reagents that can be used. These enzymes vary in target residues and strength, which change how thoroughly they digest the tissue. A stronger enzyme cocktail would be more useful in the preparation of a dense tissue such as dermal tissue, however, these enzymes have the ability to cleave residues that reside on the surface of cells.[51] Cleavage of surface proteins can confound results and decrease signal for certain proteins that are sensitive to proteolytic cleavage. Therefore, it is necessary to balance cell isolation with integrity of surface proteins.

Detailed systematic immune analysis of biomaterial and scaffold responses will further elucidate details of the foreign body response and mechanisms of immune-mediated regeneration. These results can then be leveraged to rationally design materials to specifically modulate the immune response, both the type of cells and their phenotype, thereby improving biomaterial performance and achieving new therapeutic functionalities.

Acknowledgments

The authors would like to thank the Bloomberg ~ Kimmel Institute for Cancer Immunotherapy for support; V. Beachley for guidance in materials preparation for pilot studies. This work was funded by the Maryland Stem Cell Research Fund (MSCRF), the Morton Goldberg Chair, and the Armed Forces Institute of Regenerative Medicine (AFIRM).

Disclosure Statement

J.H.E. has developed an Acellular Adipose Tissue (AAT) scaffold that is currently in clinical testing, and although not directly used in the study could benefit from its results. J.H.E. holds equity in Aegeria Soft Tissue associated with the AAT technology, the Johns Hopkins Office of Policy Coordination is managing this conflict. There are no other financial or intellectual conflicts to disclose.

References

1. Ratner, B.D., and Bryant, S.J. Biomaterials: where we have been and where we are going. Annu Rev Biomed Eng **6,** 41, 2004.
2. Langer, R., and Vacanti, J.P. Tissue engineering. Science (New York, NY) **260,** 920, 1993.
3. Sadtler, K., Singh, A., Wolf, M.T., Wang, X., Pardoll, D.M., and Elisseeff, J.H. Design, clinical translation and immunological response of biomaterials in regenerative medicine. Nat Rev Mater **1,** 16040, 2016.
4. Boyne, M.S., Silver, D.M., Kaplan, J., and Saudek, C.D. Timing of changes in interstitial and venous blood glucose measured with a continuous subcutaneous glucose sensor. Diabetes **52,** 2790, 2003.
5. Gilligan, B.C., Shults, M., Rhodes, R.K., Jacobs, P.G., Brauker, J.H., Pintar, T.J., and Updike, S.J. Feasibility of continuous long-term glucose monitoring from a subcutaneous glucose sensor in humans. Diabetes Technol Ther **6,** 378, 2004.
6. Bindra, D.S., Zhang, Y., Wilson, G.S., Sternberg, R., Thevenot, D.R., Moatti, D., and Reach, G. Design and in vitro studies of a needle-type glucose sensor for subcutaneous monitoring. Anal Chem **63,** 1692, 1991.
7. Green, R.A., Lovell, N.H., Wallace, G.G., and Poole-Warren, L.A. Conducting polymers for neural interfaces: challenges in developing an effective long-term implant. Biomaterials **29,** 3393, 2008.
8. Bauer, T.W., Geesink, R., Zimmerman, R., and McMahon, J.T. Hydroxyapatite-coated femoral stems. Histological analysis of components retrieved at autopsy. J Bone Joint Surg Am **73,** 1439, 1991.
9. Siggelkow, W., Faridi, A., Spiritus, K., Klinge, U., Rath, W., and Klosterhalfen, B. Histological analysis of silicone breast implant capsules and correlation with capsular contracture. Biomaterials **24,** 1101, 2003.
10. Anderson, J.M., Rodriguez, A., and Chang, D.T. Foreign body reaction to biomaterials. Semin Immunol **20,** 86, 2008.
11. Badylak, S.F., Valentin, J.E., Ravindra, A.K., McCabe, G.P., and Stewart-Akers, A.M. Macrophage phenotype as a determinant of biologic scaffold remodeling. Tissue Eng Part A **14,** 1835, 2008.
12. Badylak, S.F. The extracellular matrix as a biologic scaffold material. Biomaterials **28,** 3587, 2007.
13. Sadtler, K., Estrellas, K., Allen, B.W., Wolf, M.T., Fan, H., Tam, A.J., Patel, C.H., Luber, B.S., Wang, H., Wagner, K.R., Powell, J.D., Housseau, F., Pardoll, D.M., and Elisseeff, J.H. Developing a pro-regenerative biomaterial scaffold microenvironment requires T helper 2 cells. Science (New York, NY) **352,** 366, 2016.
14. Anderson, J.M. Inflammatory response to implants. ASAIO Trans **34,** 101, 1988.
15. Marchant, R.E., Anderson, J.M., and Dillingham, E.O. In vivo biocompatibility studies. VII. Inflammatory response to polyethylene and to a cytotoxic polyvinylchloride. J Biomed Mater Res **20,** 37, 1986.
16. Marchant, R.E., Miller, K.M., and Anderson, J.M. In vivo biocompatibility studies. V. In vivo leukocyte interactions with Biomer. J Biomed Mater Res **18,** 1169, 1984.
17. Marchant, R.E., Anderson, J.M., Phua, K., and Hiltner, A. In vivo biocompatibility studies. II. Biomer: preliminary cell adhesion and surface characterization studies. J Biomed Mater Res **18,** 309, 1984.
18. Marchant, R., Hiltner, A., Hamlin, C., Rabinovitch, A., Slobodkin, R., and Anderson, J.M. In vivo biocompatibility studies. I. The cage implant system and a biodegradable hydrogel. J Biomed Mater Res **17,** 301, 1983.
19. Vegas, A.J., Veiseh, O., Doloff, J.C., Ma, M., Tam, H.H., Bratlie, K., Li, J., Bader, A.R., Langan, E., Olejnik, K., Fenton, P., Kang, J.W., Hollister-Locke, J., Bochenek, M.A., Chiu, A., Siebert, S., Tang, K., Jhunjhunwala, S., Aresta-Dasilva, S., Dholakia, N., Thakrar, R., Vietti, T., Chen, M., Cohen, J., Siniakowicz, K., Qi, M., McGarrigle, J., Lyle, S., Harlan, D.M., Greiner, D.L., Oberholzer, J., Weir, G.C., Langer, R., and Anderson, D.G. Combinatorial hydrogel library enables identification of materials that mitigate the foreign body response in primates. Nat Biotech **34,** 345, 2016.
20. Mano, J.F., Sousa, R.A., Boesel, L.F., Neves, N.M., and Reis, R.L. Bioinert, biodegradable and injectable polymeric matrix composites for hard tissue replacement: state of the art and recent developments. Compos Sci Technol **64,** 789, 2004.

21. Matzinger, P., and Kamala, T. Tissue-based class control: the other side of tolerance. Nat Rev Immunol **11,** 221, 2011.
22. Matzinger, P. Friendly and dangerous signals: is the tissue in control? Nat Immunol **8,** 11, 2007.
23. Streilein, J.W. Unraveling immune privilege. Science (New York, NY) **270,** 1158, 1995.
24. Gurtner, G.C., Werner, S., Barrandon, Y., and Longaker, M.T. Wound repair and regeneration. Nature **453,** 314, 2008.
25. DiPietro, L.A. Wound healing: the role of the macrophage and other immune cells. Shock **4,** 233, 1995.
26. Gause, W.C., Wynn, T.A., and Allen, J.E. Type 2 immunity and wound healing: evolutionary refinement of adaptive immunity by helminths. Nat Rev Immunol **13,** 607, 2013.
27. Lord, J.M., Midwinter, M.J., Chen, Y.F., Belli, A., Brohi, K., Kovacs, E.J., Koenderman, L., Kubes, P., and Lilford, R.J. The systemic immune response to trauma: an overview of pathophysiology and treatment. Lancet **384,** 1455, 2014.
28. Barbul, A. Role of T-cell-dependent immune system in wound healing. Prog Clin Biol Res **266,** 161, 1987.
29. Stefater, J.A., 3rd, Ren, S., Lang, R.A., and Duffield, J.S. Metchnikoff's policemen: macrophages in development, homeostasis and regeneration. Trends Mol Med **17,** 743, 2011.
30. Chazaud, B. Macrophages: supportive cells for tissue repair and regeneration. Immunobiology **219,** 172, 2014.
31. Salmon-Ehr, V., Ramont, L., Godeau, G., Birembaut, P., Guenounou, M., Bernard, P., and Maquart, F.X. Implication of interleukin-4 in wound healing. Lab Invest **80,** 1337, 2000.
32. Aurora, A.B., and Olson, E.N. Immune modulation of stem cells and regeneration. Cell Stem Cell **15,** 14, 2014.
33. Godwin, J.W., Pinto, A.R., and Rosenthal, N.A. Macrophages are required for adult salamander limb regeneration. Proc Natl Acad Sci U S A **110,** 9415, 2013.
34. Ruffell, D., Mourkioti, F., Gambardella, A., Kirstetter, P., Lopez, R.G., Rosenthal, N., and Nerlov, C. A CREB-C/EBPbeta cascade induces M2 macrophage-specific gene expression and promotes muscle injury repair. Proc Natl Acad Sci U S A **106,** 17475, 2009.
35. Heredia, J.E., Mukundan, L., Chen, F.M., Mueller, A.A., Deo, R.C., Locksley, R.M., Rando, T.A., and Chawla, A. Type 2 innate signals stimulate fibro/adipogenic progenitors to facilitate muscle regeneration. Cell **153,** 376, 2013.
36. Brown, B.N., Sicari, B.M., and Badylak, S.F. Rethinking regenerative medicine: a macrophage-centered approach. Front Immunol **5,** 510, 2014.
37. Brown, B.N., Ratner, B.D., Goodman, S.B., Amar, S., and Badylak, S.F. Macrophage polarization: an opportunity for improved outcomes in biomaterials and regenerative medicine. Biomaterials **33,** 3792, 2012.
38. Brown, B.N., Londono, R., Tottey, S., Zhang, L., Kukla, K.A., Wolf, M.T., Daly, K.A., Reing, J.E., and Badylak, S.F. Macrophage phenotype as a predictor of constructive remodeling following the implantation of biologically derived surgical mesh materials. Acta Biomater **8,** 978, 2012.
39. Sicari, B.M., Dziki, J.L., Siu, B.F., Medberry, C.J., Dearth, C.L., and Badylak, S.F. The promotion of a constructive macrophage phenotype by solubilized extracellular matrix. Biomaterials **35,** 8605, 2014.
40. Sicari, B.M., Rubin, J.P., Dearth, C.L., Wolf, M.T., Ambrosio, F., Boninger, M., Turner, N.J., Weber, D.J., Simpson, T.W., Wyse, A., Brown, E.H., Dziki, J.L., Fisher, L.E., Brown, S., and Badylak, S.F. An acellular biologic scaffold promotes skeletal muscle formation in mice and humans with volumetric muscle loss. Sci Transl Med **6,** 234ra58, 2014.
41. Gronski, T.J., Martin, R.L., Kobayashi, D.K., Walsh, B.C., Holman, M.C., Huber, M., Van Wart, H.E., and Shapiro, S.D. Hydrolysis of a broad spectrum of extracellular matrix proteins by human macrophage elastase. J Biol Chem **272,** 12189, 1997.
42. Condeelis, J., and Pollard, J.W. Macrophages: obligate partners for tumor cell migration, invasion, and metastasis. Cell **124,** 263, 2006.
43. Beachley, V.Z., Wolf, M.T., Sadtler, K., Manda, S.S., Jacobs, H., Blatchley, M.R., Bader, J.S., Pandey, A., Pardoll, D., and Elisseeff, J.H. Tissue matrix arrays for high-throughput screening and systems analysis of cell function. Nat Methods **12,** 1197, 2015.
44. Dreifuss, S.E., Wollstein, R., Badylak, S.F., and Rubin, P.J. Acellular micronized extracellular matrix and occlusive dressings for open fingertip injuries. Plast Aesthetic Res **2,** 282, 2015.
45. Reznichenko, A. Different biologic grafts for diaphragmatic crura reinforcement during laparoscopic repair of large hiatal hernia: a 6-year single surgeon experience. J Med Imp Surg **1,** 2, 2015.
46. Allman, A.J., McPherson, T.B., Badylak, S.F., Merrill, L.C., Kallakury, B., Sheehan, C., Raeder, R.H., and Metzger, D.W. Xenogeneic extracellular matrix grafts elicit a TH2-restricted immune response. Transplantation **71,** 1631, 2001.
47. Allman, A.J., McPherson, T.B., Merrill, L.C., Badylak, S.F., and Metzger, D.W. The Th2-restricted immune response to xenogeneic small intestinal submucosa does not influence systemic protective immunity to viral and bacterial pathogens. Tissue Eng **8,** 53, 2002.
48. East, L., and Isacke, C.M. The mannose receptor family. Biochim Biophys Acta **1572,** 364, 2002.
49. Gazi, U., and Martinez-Pomares, L. Influence of the mannose receptor in host immune responses. Immunobiology **214,** 554, 2009.
50. Stewart, M., Thiel, M., and Hogg, N. Leukocyte integrins. Curr Opin Cell Biol **7,** 690, 1995.
51. Zhang, B., Shan, H., Li, D., Li, Z.R., Zhu, K.S., Jiang, Z.B., and Huang, M.S. Different methods of detaching adherent cells significantly affect the detection of TRAIL receptors. Tumori **98,** 800, 2012.

Address correspondence to:
Jennifer H. Elisseeff, PhD
Translational Tissue Engineering Center
Department of Biomedical Engineering
Johns Hopkins University School of Medicine
5031 Smith Building
400 North Broadway
Baltimore, MD 21231

E-mail: jhe@jhu.edu

Received: August 3, 2016
Accepted: September 23, 2016
Online Publication Date: November 9, 2016